CERN – EUROPEAN ORGANIZATION FOR NUCLEAR RESEARCH

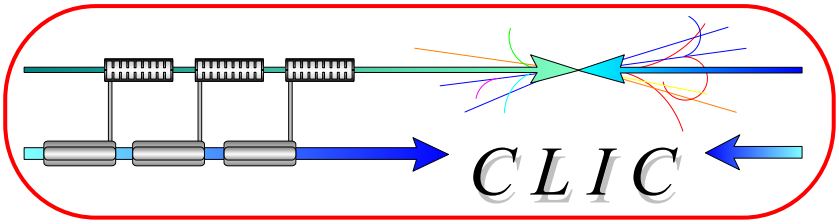

CLIC Note 657

OPERATIONAL EXPERIENCE WITH A CID CAMERA SYSTEM

C.P. Welsch, E. Bravin, B. Burel, T. Lefèvre

Abstract

In future high intensity, high energy accelerators particle losses must be minimized as activation of the vacuum chambers or other components makes maintenance and upgrade work time consuming and costly. It is imperative to have a clear understanding of the mechanisms that can lead to halo formation, and to have the possibility to test available theoretical models with an adequate experimental setup.

Measurements based on **o**ptical **t**ransition **r**adiation (OTR) provide an interesting opportunity for analyzing the transverse beam profile due to the fast time response and very good linearity of the signal with respect to the beam intensity. On the other hand, the dynamic range of typical acquisition systems as they are used in the **C**LIC **t**est **f**acility (CTF3) is typically limited and must be improved before these systems can be applied to halo measurements. One possibility for high dynamic range measurements is an innovative camera system based on **c**harge **i**njection **d**evice (CID) technology.

With possible future measurements in CTF3 in mind, comparative measurements performed with this innovative camera system, a standard CCD camera and a step-by-step measurement technique based on a small photomultiplier are summarized with emphasis on the operational experience with the CID camera system.

Geneva, Switzerland
26/4/2006

OPERATIONAL EXPERIENCE WITH A CID CAMERA SYSTEM

C.P. Welsch, E. Bravin, B. Burel, T. Lefèvre
CERN, Geneva, Switzerland

Abstract

In future high intensity, high energy accelerators particle losses must be minimized as activation of the vacuum chambers or other components makes maintenance and upgrade work time consuming and costly. It is imperative to have a clear understanding of the mechanisms that can lead to halo formation, and to have the possibility to test available theoretical models with an adequate experimental setup.

Measurements based on **o**ptical **t**ransition **r**adiation (OTR) provide an interesting opportunity for analyzing the transverse beam profile due to the fast time response and very good linearity of the signal with respect to the beam intensity. On the other hand, the dynamic range of typical acquisition systems as they are used in the **C**LIC **t**est **f**acility (CTF3) is typically limited and must be improved before these systems can be applied to halo measurements. One possibility for high dynamic range measurements is an innovative camera system based on **c**harge **i**njection **d**evice (CID) technology.

With possible future measurements in CTF3 in mind, comparative measurements performed with this innovative camera system, a standard CCD camera and a step-by-step measurement technique based on a small photomultiplier are summarized with emphasis on the operational experience with the CID camera system.

INTRODUCTION

In spite of its central importance for all future high intensity accelerators, very few dedicated experimental approaches have been attempted in order to understand the mechanism of beam halo formation [1, 2, 3].

Profile measurements based on optical techniques like synchrotron radiation [see e.g. 4, 5], optical transition radiation (OTR) [6, 7] or diffraction radiation [8, 9] are today established as reliable and precise techniques that are widely used in the field of accelerators. OTR is an especially interesting candidate for halo measurements since it not only provides a visible wavelength signal linear with the bunch charge over a wide range, but also it offers a spatial resolution down to the μm range and thus covers the requirements at CTF3 [10, 11, 12]. The number of OTR photons N_{OTR} that are created within a specific wavelength interval between λ_a and λ_b at a beam energy γ is given by [6]

$$N_{OTR} = \frac{2\alpha}{\pi} \ln\left(\frac{\lambda_b}{\lambda_a}\right)\left[\ln(2\gamma) - 1/2\right] \qquad (1)$$

where the fine structure constant $\alpha = e^2/(\hbar c) \approx 1/137$ was used.

With beam energies of approximately 10 MeV, the yield (N_{OTR}) is around $1 \cdot 10^{-3}$ in the visible range [400 nm; 600nm]. With a number of 10^{10} electrons per bunch and beam energies

up to 150 MeV available at CTF3, a halo monitor will require a dynamic range of $10^4 – 10^5$ in order to be able to benchmark and improve upon existing theoretical models.

The typical apparatus in CTF3 as shown in Figure 1 is composed of a set of achromatic lenses, mirrors, optical density filters, and a standard CCD camera with 8-bit digitization. It is obvious that the CCD camera with 8-bit digitization clearly limits the overall performance, and does not give access to halo measurements with the necessary dynamic range. Even though high dynamic range CCD cameras are available on the market (see e.g. [13]), they are very expensive. An interesting alternative is the SpectraCAM® camera system available from Thermo Electron Corporation [14]. Other possible approaches include masking part of the beam [15] or using multi mirror arrays to deflect the intense central part of the beam and limit the measurement to the weaker tail regions of the light distribution [16].

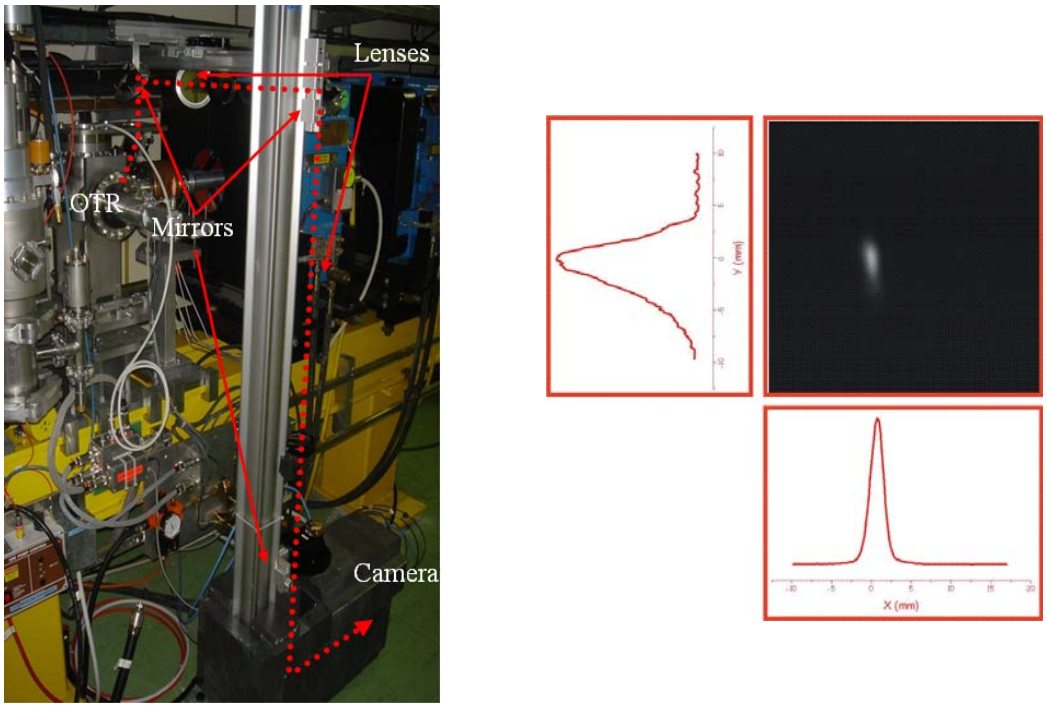

Figure 1: Overview of a standard OTR-based profile measurement system and a typical measurement at CTF3.

Although it was invented more than two decades ago by G. Michon at General Electric [17], and although it offers a number of interesting advantages in direct comparison to CCD cameras, CID technology is still not widely used in the field of particle accelerators. The "charge injection device (CID)" derives its name from its unique ability to clear individual pixel sites of photon-generated charge by *injecting* the charge directly into the substrate. The main features of this imager technology are its distinctive readout capabilities including inherent resistance to ionizing radiation, inherent resistance to charge blooming, true random pixel addressability, non-destructive pixel readout (NDRO), and on-sensor collective pixel readout and clear. The on-sensor collective read feature allows the data acquisition routines to select contiguous pixel regions (e.g., a 3 by 3 pixel region) and interrogate those pixels with a single reading that is the electronic average of the signals on those pixels, thereby improving both readout speed and signal-to-noise ratio. This collective read feature is analogous to the 'binning' that can be performed with certain CCD camera systems.

However, unlike the CCD where the charge packets from the individual pixels are physically combined into a single larger charge packet, the CID collective read feature preserves the spatial integrity of the photon-generated charge in the pixels and the read process is non-destructive to that charge. The CID architecture also allows for the clearing of photon-generated charge from contiguous pixel regions with a single 'inject' pulse.

Similar to most micro-electronic devices built today, the CID is manufactured with silicon technology. A single crystal silicon wafer forms the substrate of the device. The insulating Si substrate is doped with boron to make it electrically conductive (p-type). Upon the substrate, an n-doped epitaxial layer is grown. As the thickness of the epitaxial layer is increased, the full well capacity and NIR response also increase. The epitaxial layer is slightly doped in such a manner as to cause minority signal carrier diffusion into the bulk silicon. Next, a thick field oxide is grown in a checker board pattern across the surface of the wafer. The field oxide is an isolating layer, a dielectric film, composed of silicon dioxide. A thin gate oxide of about 400 nm of SiO_2, is grown over the remaining exposed epitaxial layer. Conductive poly-silicon is then applied in thin strips that regularly crisscross the entire surface of the imager forming the row and column electrodes. The two orthogonal poly-silicon electrodes are electrically isolated and connect pixels to the processing electronics at the periphery of the device. One electrode is designated the column or "sense" electrode and the other is the row or "drive" electrode. The region at the intersection of the two electrodes under the thin gate oxide delineates the active charge-storage area for each pixel. An overview of a single pixel is given in Figure 2.

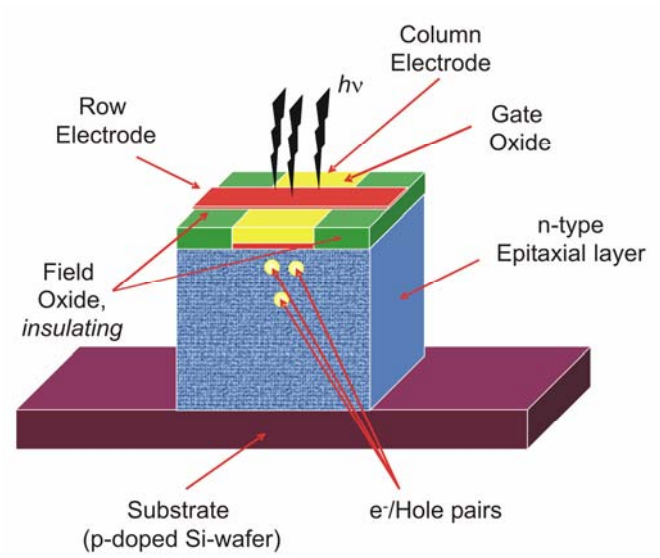

Figure 2: Schematic view of a single pixel on the CID imager.

Each pixel on the CID imager is individually addressable and allows for random access non-destructive pixel readout. This feature is illustrated in Figure 3. During image acquisition, the photon-generated charge is typically stored under the row (or drive) electrode (see stage 1). In order to determine the level of accumulated charge, the column (or sense) electrode is allowed to float, and the 1st voltage sample is taken on the electrode (see stage 2). Next, the row (or drive) electrode voltage is collapsed thereby causing the photon-generated charge to transfer to the column (or sense) electrode. At this point, the 2nd voltage sample is acquired (see stage 3).

The voltage difference between the 2nd voltage sample and the 1st voltage sample is proportional to the amount of photon-generated charge at the pixel site. At this point, the column and row electrodes may be returned to their original bias conditions allowing for the continued integration of photon-generated charge (see stage 1), or alternatively, the voltages on both electrodes can be collapsed thereby causing the pixel to be cleared of charge (see stage 4). As demonstrated in Figure 3, photon-generated charge may be transferred within each individually addressable pixel for readout without actually destroying the charge – a clear advantage in comparison to any other camera technique.

Another interesting feature of the chip is that the CID pixel structure is inherently anti-blooming, which eliminates the axial smear or radial blooming caused by an intensely illuminated pixel on many CCD camera systems.

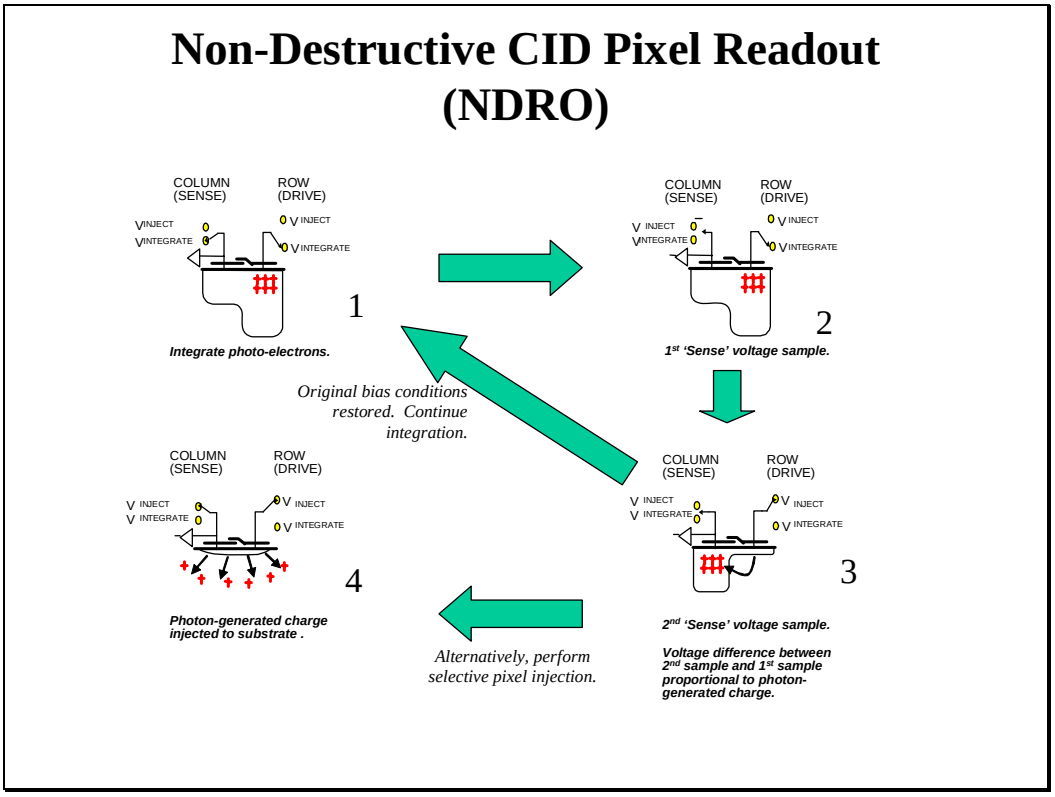

Figure 3: CID readout process and charge return.

The camera itself consists of a thermo-electrically cooled imager contained in a purged housing to which three different printed circuit boards are attached as shown in Figure 4. In addition, a recirculation cooling system, used for dissipating heat from the backside of the thermo-electric cooling stack, allows the imager to operate at a controlled temperature of -30°C. This reduces dark current and the attendant dark current shot noise thereby optimizing signal-to-noise ratio. Finally, the camera includes a *support package* that incorporates power supplies and a molecular sieve trap to purify the purge gas. The three printed circuit boards attached to the camera housing are: (1) A custom made Analog Signal Processing (ASP) board that digitizes the video signal from the CID imager to 16 bits of precision. (2) A

custom made Timing Signal Processing (TSP) board that incorporates a Flex Altera® gate array to drive the CID imager, and (3) a commercially available JumptecAdastra (Switzerland) MOPSLCD6 embedded CPU that employs a 266 MHz Pentium processor, 100 MBit Ethernet connectivity to a host PC, and 128 MB RAM (expandable) on board.

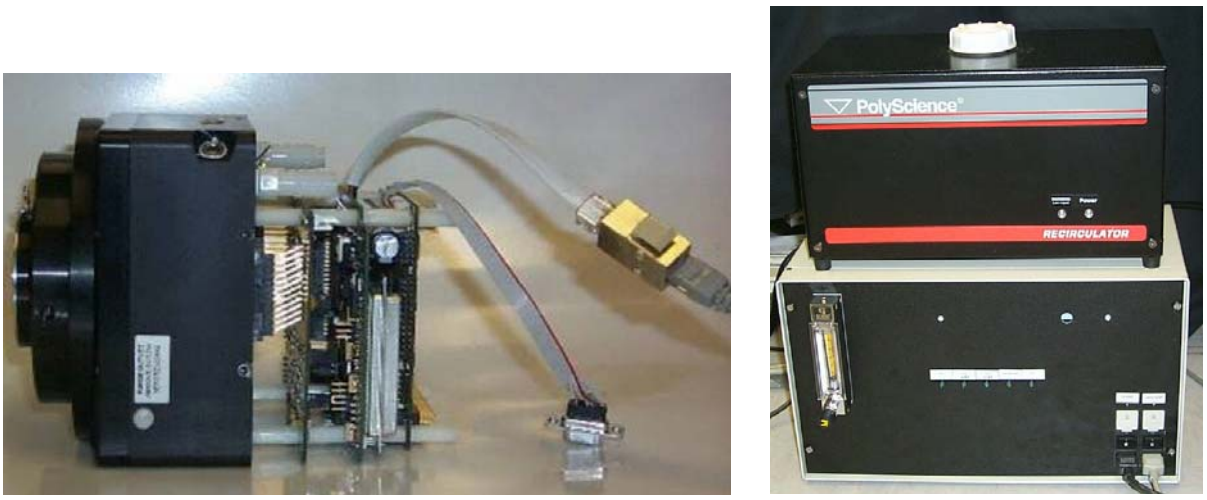

Figure 4: Photographs of the CID camera with the attached data acquisition cards and the "support package", used for data integration and cooling of the chip.

As is readily apparent in Figure 4, the overall camera apparatus is not extremely radiation hard despite the inherent radiation resistance of the CID imager itself. Any such CID camera system installed in an environment like CTF3 must be appropriately shielded.

The CID detector provides high quantum efficiency over a wide wavelength range, and is able to cover applications requiring adequate quantum efficiency from the NIR (< 1000 nm) to UV (> 150 nm) as depicted in Figure 5. Even though this is not of particular importance for its application to accelerator diagnostics in CTF3, broad range quantum efficiency is clearly a general advantage of CID detection in comparison to CCD detection.

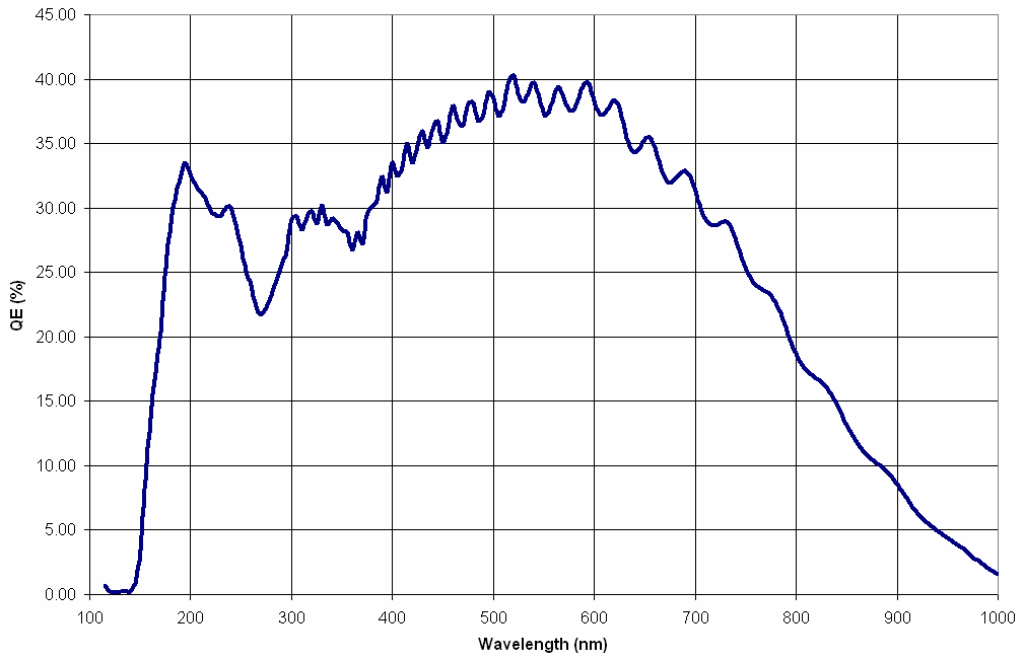

Figure 5: Quantum efficiency of the CID chip as a function of the wavelength of the incident photons.

CID DATA ACQUISITION MODES

The camera is controlled via its Ethernet interface from a Windows® workstation that is not only used to control image acquisition, but also provides direct access to most of the camera operating parameters on a level as detailed as the drive voltages for the individual pixels. Different acquisition modes can be used and are discussed in the following section.

Fixed Time Mode

The Fixed Time acquisition mode is analogous to a standard image acquisition on a CCD camera. First, the user defines the exposure time for an individual user-defined sub-array (Xo, Yo, dX, and dY) or for multiple user-defined sub-arrays. In contrast to CCD imagers, the sub-array doesn't necessarily have to comprise the entire area of the imager, but rather it could be any rectangular array of pixels, ranging down to a single pixel.

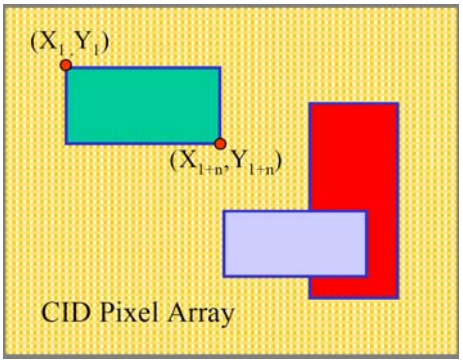

Figure 6: Possible array definitions on the CID chip.

Using the unique readout features of the CID chip, these arrays can overlap, and may even be assigned different exposure times, Figure 6. The maximum number of sub-arrays to be exposed is not limited by the software, but is usually a relatively low number (< 10).

Time Resolved Mode

The Time Resolved acquisition mode provides signal versus time information on user-defined regions of interest. The resulting signal profiles versus time may be plotted in integral, 1st derivative, or 2nd derivative mode. The rate of data acquisition is user programmable and can range from as low as 10 milliseconds up to several seconds per point depending on the size of the user-defined regions of interest and the total duration of the exposure. This Time Resolved mode is ideal for the initial setup of an experiment as it allows the user to make real-time adjustments to the apparatus to optimize signal-to-noise ratio. For example, by adding optical density filters in real-time in front of the camera, direct control and optimization of the light level impinging on the CID imager is feasible.

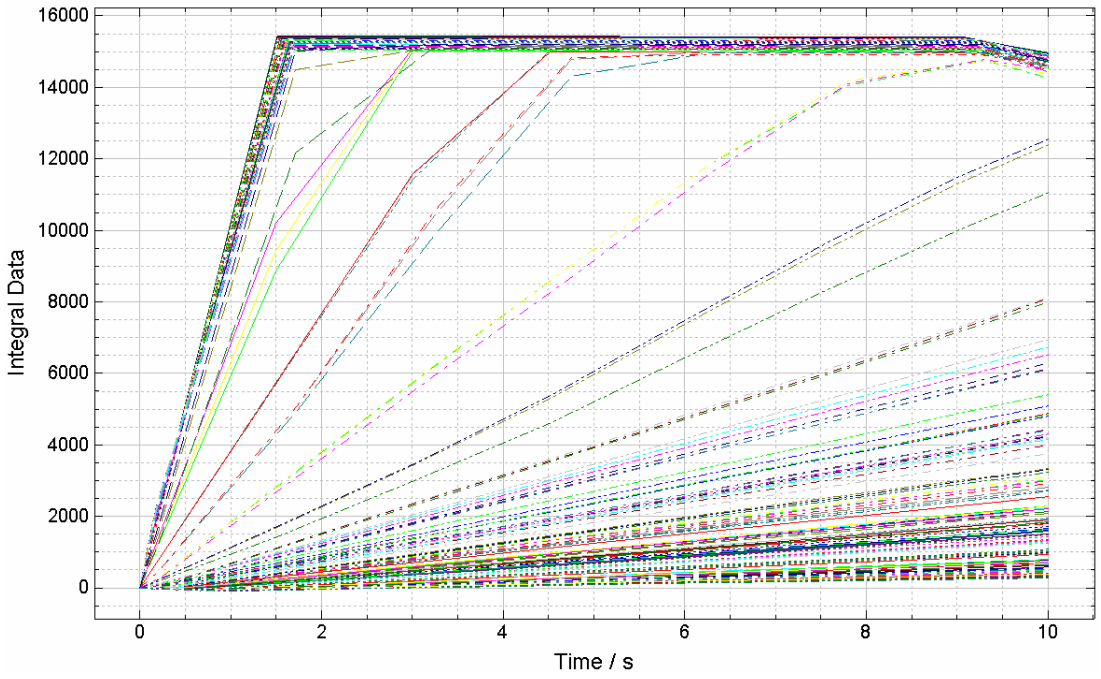

Figure 7: Example of a time resolved measurement. The plot shows the evolution of the number of photons per pixel as a function of time.

One important limitation of this mode results from memory limitations on the CPU board. For example, consider a beam that covers a large area on the imager i.e. a circular region 512 pixels in diameter. Taking advantage of the assumed symmetry of the source, i.e. a round electron beam, one would typically limit the acquisition to one radial direction. In the case where time dependent information is required for each single pixel across the beam profile, one ends up with a total number of 512 sub-arrays that need to be readout continuously. With an overall exposure time of 10 seconds and a required time resolution of 0.1 seconds the algorithms must acquire a total number of 100 time points per pixel plus a camera-defined number of 500 extra

points, yielding a total number of 307,200 points. Each point will require a memory block of 364 Bytes to store the information. Thus, the total memory requirement for a total number of only 512 pixels adds up to 307,000 x 364 Byte = 111 MByte, which is already close to the 128-Mbyte memory limit on the CPU. Time Resolved measurement must, therefore, be limited to both a reasonable number of sub-arrays and data acquisition rate (points per second) given the memory constraints.

Random Access Integration

The CID acquisition mode that provides the most benefit for this work is the Random Access Integration (RAI) mode. In RAI mode, the user defines a maximum exposure time and one or more sub-arrays of interest defined with a horizontal origin (Xo), a vertical origin (Yo), a horizontal size (dX) and a vertical size (dY). The user may also define a desired 'binning' resolution (Xbin, Ybin). For example, a user could define a sub-array as follows: Xo = 345, Yo = 128, dX = 15, dY = 3, Xbin = 1, and Ybin =3. (Note that for this beam profiling application, the Xbin and Ybin values are set to 1 in order to maximize image resolution.) For this example, whenever it is necessary for the algorithms to interrogate this sub-array, 15 readings would be acquired with a 1 by 3 binning pattern starting at the ROI origin (Xo = 345, Yo = 128). In addition to the overall sub-array, the user must also define a 'Control Region,' which is typically smaller than the overall sub-array and includes the most intensely illuminated pixel, *Figure 8*. In the example listed here, the 'Control Region' could be a 3 by 3 pixel area in the middle of the ROI (Xo = 351, Yo = 128, dX = 3, and dY = 3). The RAI algorithms sequentially observe the 'Control Regions' for all of the user-defined sub-arrays in a circular queue. Whenever the signal on the 'Control Region' reaches a threshold signal level (typically defined as 75% of full well capacity), the entire sub-array is read, the data is stored in the camera memory, and finally the pixels in the sub-array are reset (injected) and a new integration cycle is begun. Each sub-array is cycled as many times as necessary until the user defined maximum exposure time expires. These RAI algorithms dramatically extend dynamic range because the maximum observable signal is not limited by one full well capacity, but rather it is limited by the number of times the sub-array can be cycled given the user defined maximum exposure time. In many applications, the sub-array can be cycled tens or hundreds of thousands of times in the user defined exposure period thereby extending dynamic range by 3 or 4 orders of magnitude. The cycle time from 0 to the threshold signal is automatically adjusted from sub-array to sub-array based upon the real-time observation of the signal accumulation rate on the 'Control Region.'

There are limits to the RAI mode. The maximum cycle frequency of a sub-array, which in turn limits the maximum achievable dynamic range, depends on numerous factors including: the total number of user defined sub-arrays win the RAI circular queue, the number of pixels in each sub-array, whether or not binning is employed, camera readout frequency (either 50 kHz or 200 kHz with the SpectraCAM®), and the illumination level on the user defined subarrays. For these beam profile experiments, the dynamic range could be further improved by disregarding the central region of the beam and simply limiting the observations to the halo regions of the light distribution by defining sub-arrays only in those regions.

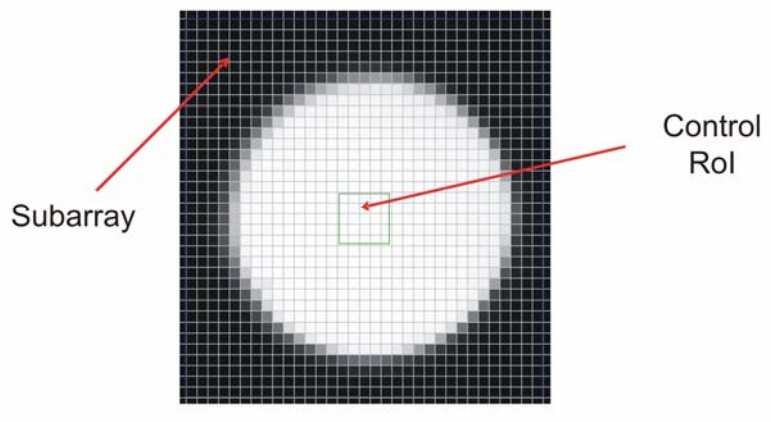

Figure 8: Detailed view of one sub-array and the definition of the Control ROI.

True random pixel addressability guarantees that individual pixels may be read out in a random fashion, not necessarily in a structured progressive pixel by pixel, line by line format. The ability to read out pixels in this manner permits the read out of pixels of interest whereby extraneous information is ignored. Hence, relevant information is obtained at faster effective frame rates and less data has to be interpreted by the computer processing system.

In order to reduce the effective camera system noise thereby improving signal-to-noise ratio, up to 128 non-destructive reads (NDROs) are automatically employed on weakly illuminated pixels in RAI mode. Since camera system noise is typically white noise, the effective read noise of the camera system reduces proportionally to the square root of the number of NDROs, Figure 9. This further extends the dynamic range of the camera system in weakly illuminated regions of the field of view.

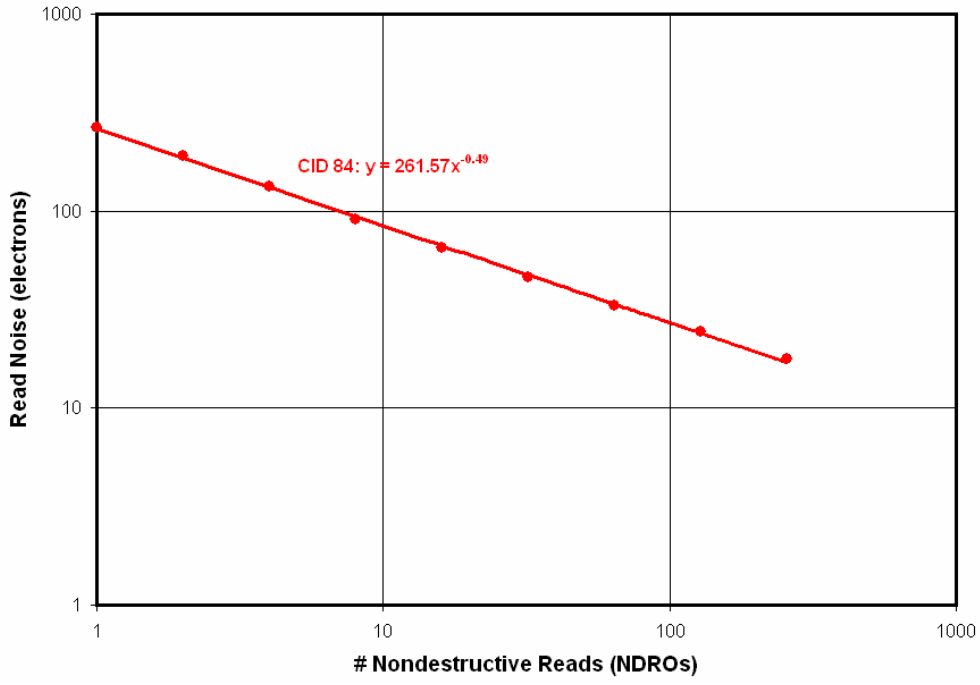

Figure 9: Read noise of the SpectraCAM® system as a function of non-destructive readouts.

SOFTWARE PACKAGE

The *RACID Exposure* software that accompanies the SpectraCAM^{TM} system is able to control most of the camera parameters directly via an Ethernet interface. It should be noted that the present version of the graphical user interface software is in a β-state, since not only the documentation is incomplete, but also bugs in the interface code leads to regular system hang-ups and subsequent reboots of the entire system. Both the camera and the software are designed specifically to ease the integration of the camera into instrumentation products produced by original equipment manufacturers (OEM) and thus the focus of Thermo Electron continues to be OEM customer support rather than the finalization of the graphical user interface software. The low-level camera interface libraries and the data acquisition firmware are in a complete state since these modules are used extensively by Thermo Electron's OEM customers. At the present stage, many of the advanced camera features are not clearly explained in the documentation. New camera control and data acquisition software must be developed for future applications of the camera system in CTF3.

However, the software does already give access to most of the camera features and thus allowed test measurements with all the different image acquisition modes. Definition of the exposure array and integrated sub-arrays is straight forward: One defines the starting points in x- and y-directions (Xo and Yo) and the extent of the sub-array in each dimension (dX and dY). Exposure times can be entered globally for all defined sub-arrays, or separately for each of the sub-array independently. The size (dX and dY) of the sub-arrays is not limited and can range from a single pixel to the entire imager surface. Other shapes, like "donut-like" exposure regions as would be desirable for beam halo measurements have to be entered pixel-by-pixel as no tools for the definition of more complex sub-array shapes exist.

In all measurements described here, the factory settings for the cameras system have been employed.

TEST MEASUREMENTS

Mille Luce M1000

In order to become familiar to the operation of the CID camera and to judge its performance, a test setup as shown in Figure 10 was installed in our optical lab. A homogeneous light source, type *MilleLuce M1000*, is introduced into a small metallic box in front of which different optical density filters from OD1 – 4 are placed to generate a well known initial light distribution.

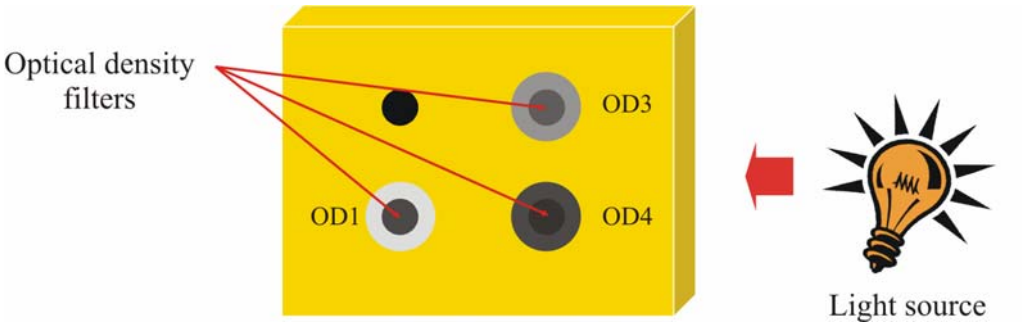

Figure 10: Schematic view of the test setup.

With this apparatus, the light source provided well defined signal geometry on the CID imager with a dynamic range of the signal of four orders of magnitude. No special care was taken to shield the background light or reduce stray light.

First, image acquisition was done in RAI mode with four different sub-arrays defined at each of the four optical density filter light spots. As indicated above, in RAI mode, the cycle time from 0 to threshold signal for each of the four sub-arrays was independent of the others and optimized based upon the experimental observation of light intensity (i.e., photon flux).

The result in the form of a three dimensional plot is shown in the following Figure 11.

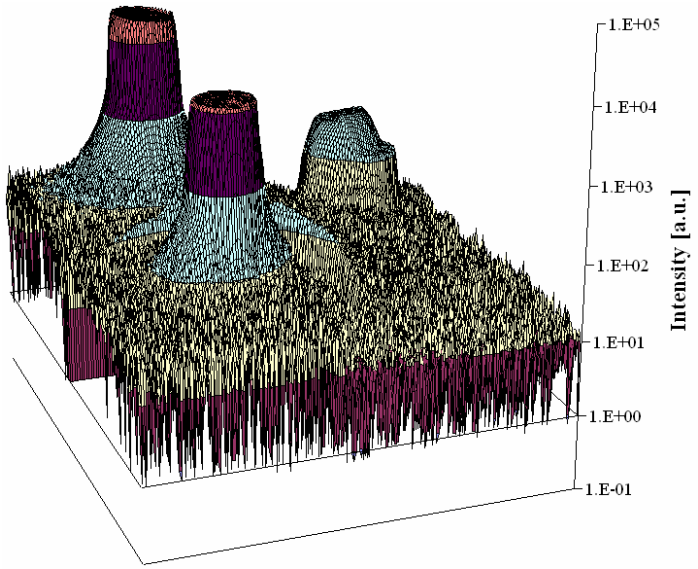

Figure 11: 3D representation of the measured intensity distribution in RAI mode for an exposure time of 1 second.

It can clearly be seen that the signal-to-noise level in this measurement was not high. This was caused by two experimental shortcomings. First, due to the fact that no shielding of background light was attempted, background noise was high. Second, the sizes of the sub-arrays established around each of the optical density filter spots were quite large. RAI mode provides optimum results and higher dynamic range when the sub-arrays it operates on are less extensive. Even though it was still possible to cover three orders of magnitude with this

simple measurement, the region covered by the OD4 filter was not distinguishable from the background noise level.

In a second experiment, observation was limited to the radial intensity distribution in each of the four optical density filter spot sections, rather than complete sub-arrays surrounding the spots. No other changes to the experimental setup were executed.

For this purpose, the *RACID Exposure* software offers the *Spectrum Draw* tool. With this feature, a large number of RAI mode sub-arrays with a width of 1 pixel column and a height of 3 pixel rows are automatically placed adjacent to one another across the radial profile of each optical density filter light spot. This large number of adjacent sub-arrays is automatically created by two simple mouse clicks that define a horizontal line along which the sub-arrays are oriented. Each of the sub-arrays is then treated in RAI mode, and thus RAI mode cycle time (i.e., dynamic range) optimization is done on the smallest possible scale, namely single pixel columns.

As can be seen in Figure 12, a dynamic range of 10^4 is covered using this *Spectrum Draw* mode. Given the extremely simple experimental setup and short exposition time, this experiment provides a good indication of the camera's dynamic range performance.

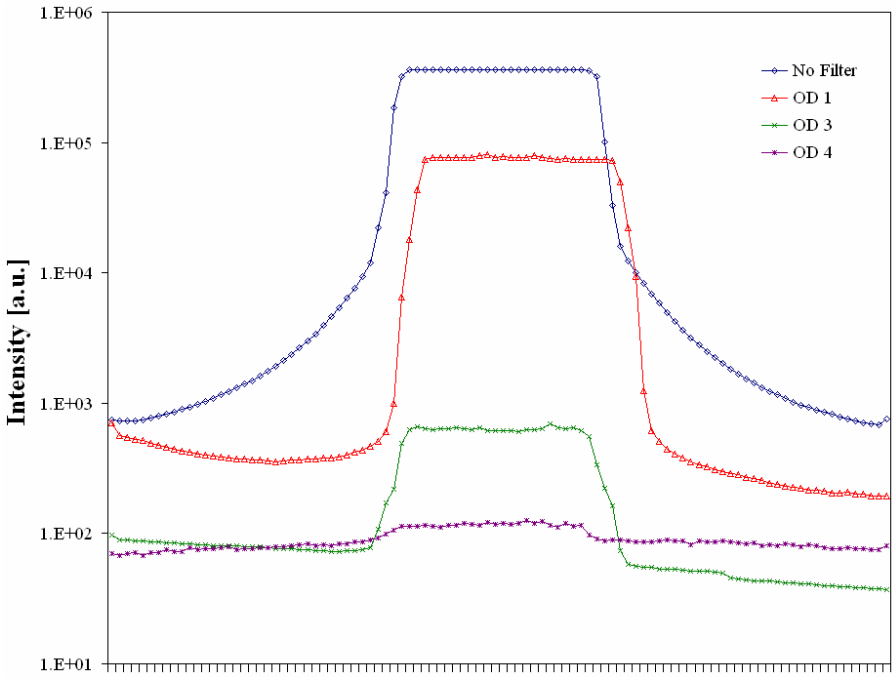

Figure 12: Measured intensity distribution in the four regions using the "spectrum draw" tool.

Pulsed Picoquant PDL 800-B laser

To enhance this performance and to simultaneously work with a light distribution that comes closer to what is expected in CTF3, the light source was exchanged with a pulsed Picoquant PDL 800-B laser. Again, the *Spectrum Draw* routine provides the ideal tool for high dynamic range measurement of this stationary light source. The measured intensity distribution along one of the main axes of the laser spot is shown in Figure 13.

It should be noted that the intensity distribution in the central region (i.e. where the pixels would saturate in milliseconds or less were it not for the RAI acquisition routines), no blooming of is observed. On the other hand, even the shortest exposure times of only 10 milliseconds do reproduce this part of the intensity distribution with high accuracy. The benefit from longer acquisition times can be seen in the tails of the distribution, where longer exposures greatly enhance the signal-to-noise ratio. With these longer exposure times, it is possible to achieve dynamic ranges of up to 10^7 with an intense pulsed laser.

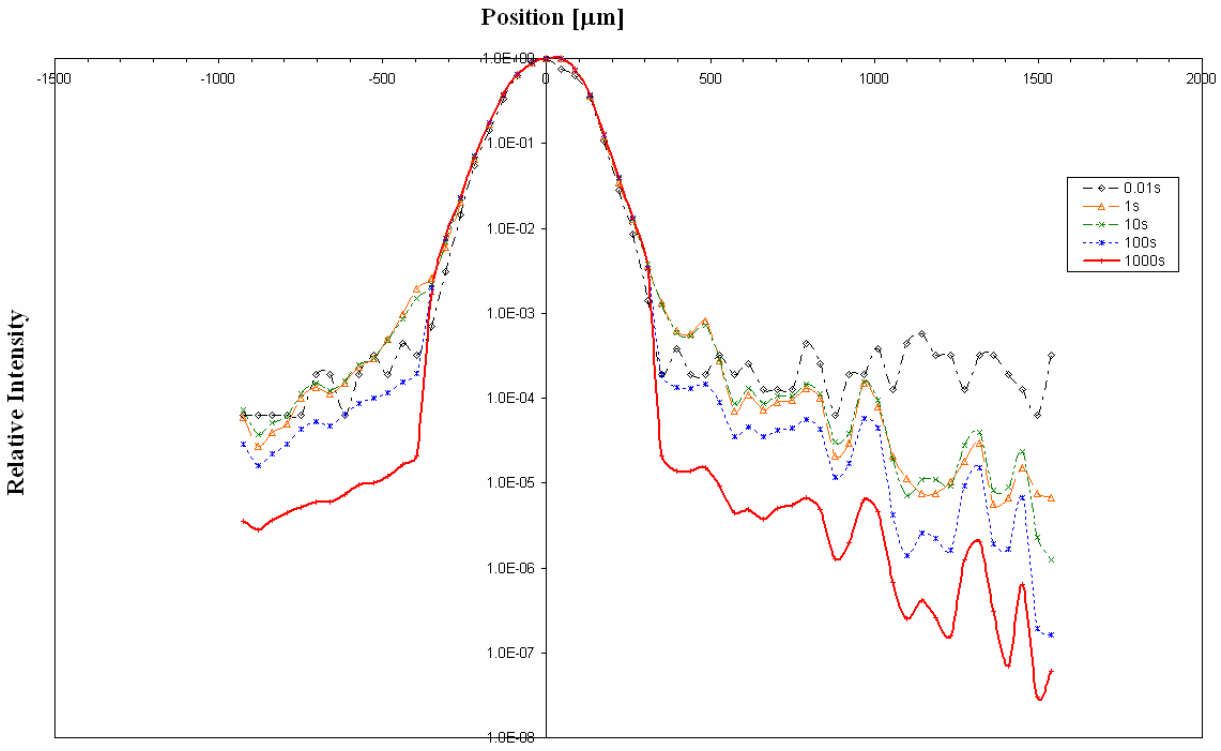

Figure 13: Relative intensity distribution of the Picoquant PDL 800-B laser as measured with the CID camera with different exposure times.

The same laser was then used for direct illumination of the CCD camera. As can be seen in *Figure 14*, the intensity of the laser was high enough to saturate the entire imager area if no optical density (OD) filter was used. By adding different filters to the setup, the light intensity in the measurements was decreased by steps of a factor of ten, and the intensity distributions were extracted from these images.

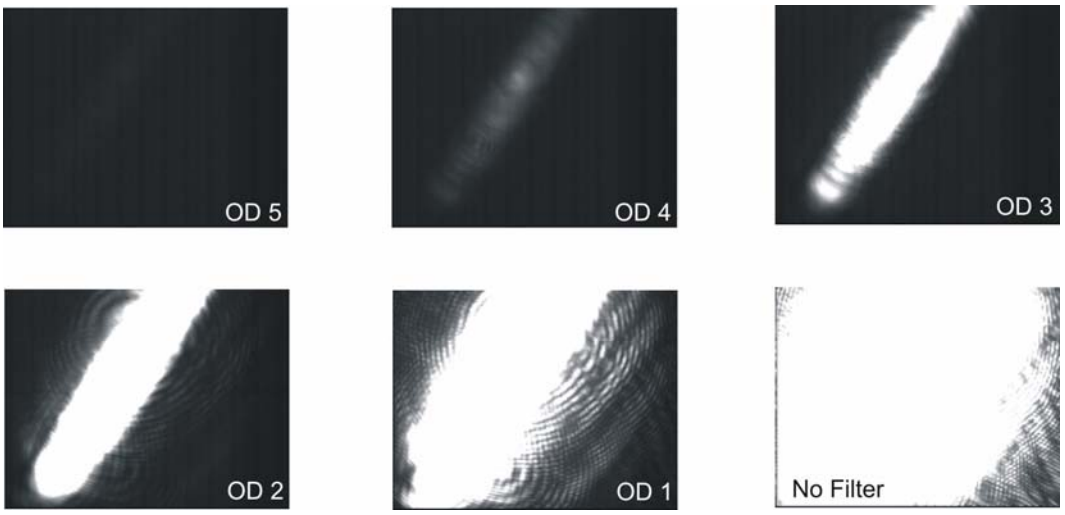

Figure 14: Laser profile as measured with the CCD camera in combination with five different optical density filters

The extracted intensity distributions along one of the main axes are shown in Figure 15. Prior to normalization, the base noise was subtracted from each pixel.

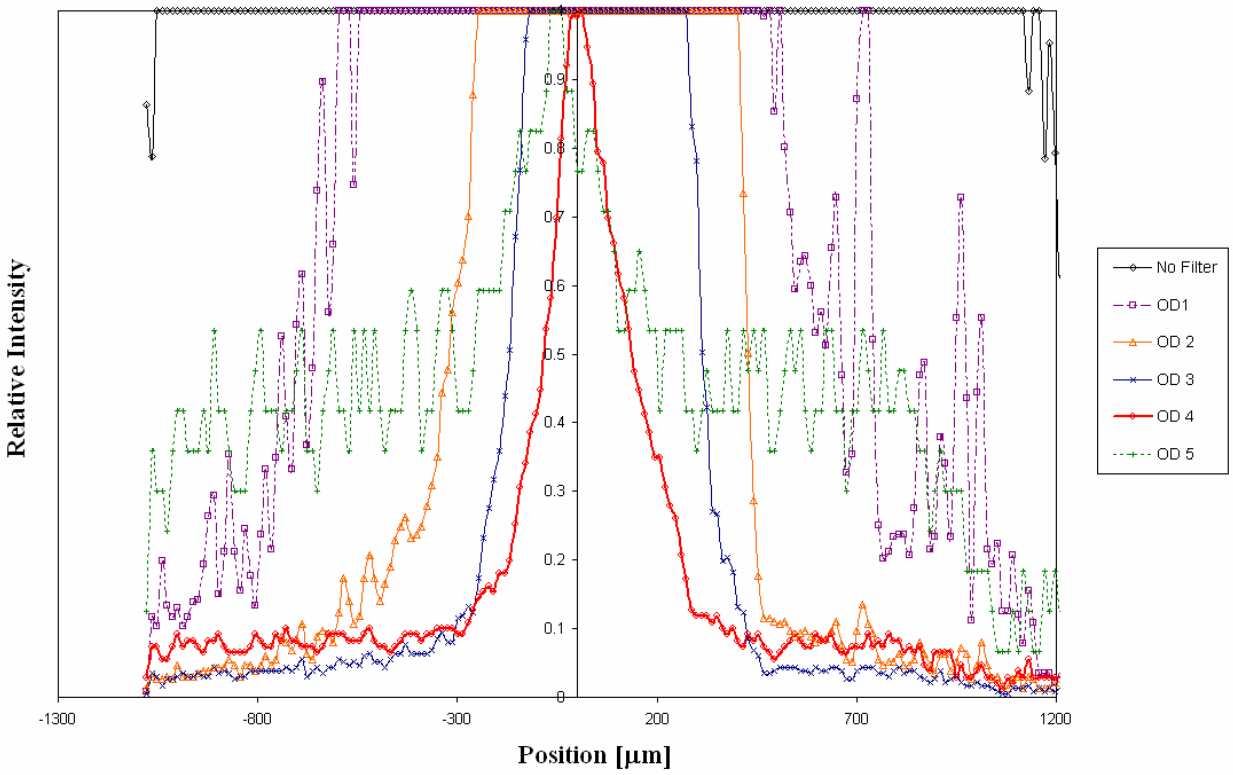

Figure 15: Relative intensity distribution as a function of the radial position for each of the measured laser profiles shown in Figure 14.

From the plot in *Figure 15*, it can be seen that for an optimum measurement, the OD4 filter should be employed, since saturation of the imager occurs only at the very centre pixels. Using the values obtained in this measurement, a Gaussian distribution can be fit to the measurements, yielding to a characteristic description of the laser beam.

COMPARISON WITH ALTERNATIVE METHODS

In order to have a comparative measurement to the CID camera that also covers a dynamic range in the order of 10^4 or better, a step-by-step acquisition system was constructed and used for preliminary tests in the optical lab. In this setup, a small Hamamatsu photomultiplier tube (PMT) type R7400U [18] was installed in a metallic box with a circular aperture ranging from 0.5 mm to 2 mm in diameter. The step size for each individual measurement was 100 μm, and thus a de-convolution of the initial data was performed to ensure comparability to the measurements from the CCD and CID cameras. However, it should be noted that the size of the aperture still leads to a signal averaging aberration because the aperture is large in comparison to the absolute pixel sizes of both the CCD and the CID cameras. The system as it is shown in Figure 16 was installed in CTF3 and will be used for tests with the particle beam in the near future.

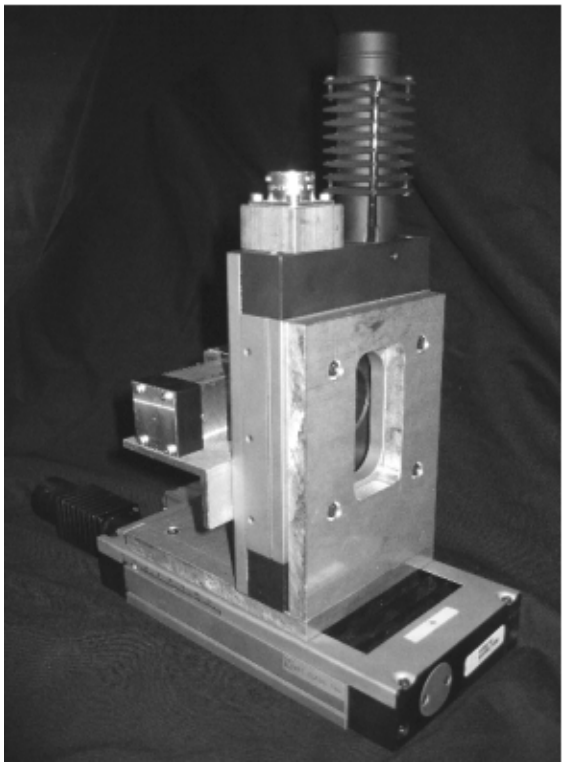

Figure 16: Photograph of the step-by-step PMT acquisition system

For the purpose of a comparative measurement, an Opto Electronics PLS20 pulsed diode laser was used. The result of the measurements with all three acquisition techniques is shown in Figure 17. While the data for all three techniques are in substantial agreement in the central beam region, the maximum achievable dynamic range of the CCD camera used here is limited to about two orders of magnitude. The PMT setup clearly improves on that situation, covering five orders of magnitude. The averaging effect caused by the size of the scanning hole can clearly be seen in the plot. By choosing a different photomultiplier tube with a

higher amplification of the signal and optimizing on the size and shape of the central aperture in the mask, one could possibly extend the dynamic range further with the PMT apparatus. For the envisaged measurements in CTF3, the demonstrated dynamic range covers the required signal levels.

The highest dynamic range and best results were achieved with the CID camera, where the maximum exposure time was set to ten minutes, which is still a reasonable time from a practical point of view – e.g. the energy resolved measurements in the spectrometer lines by step-by-step measurements with e.g. the slit dump take about the same time. Due to the limited dynamic range of the CCD on one hand, and the signal averaging aberration of the PMT setup on the other, the measurement with the CID camera showed a number of details that were not observable with the other two methods.

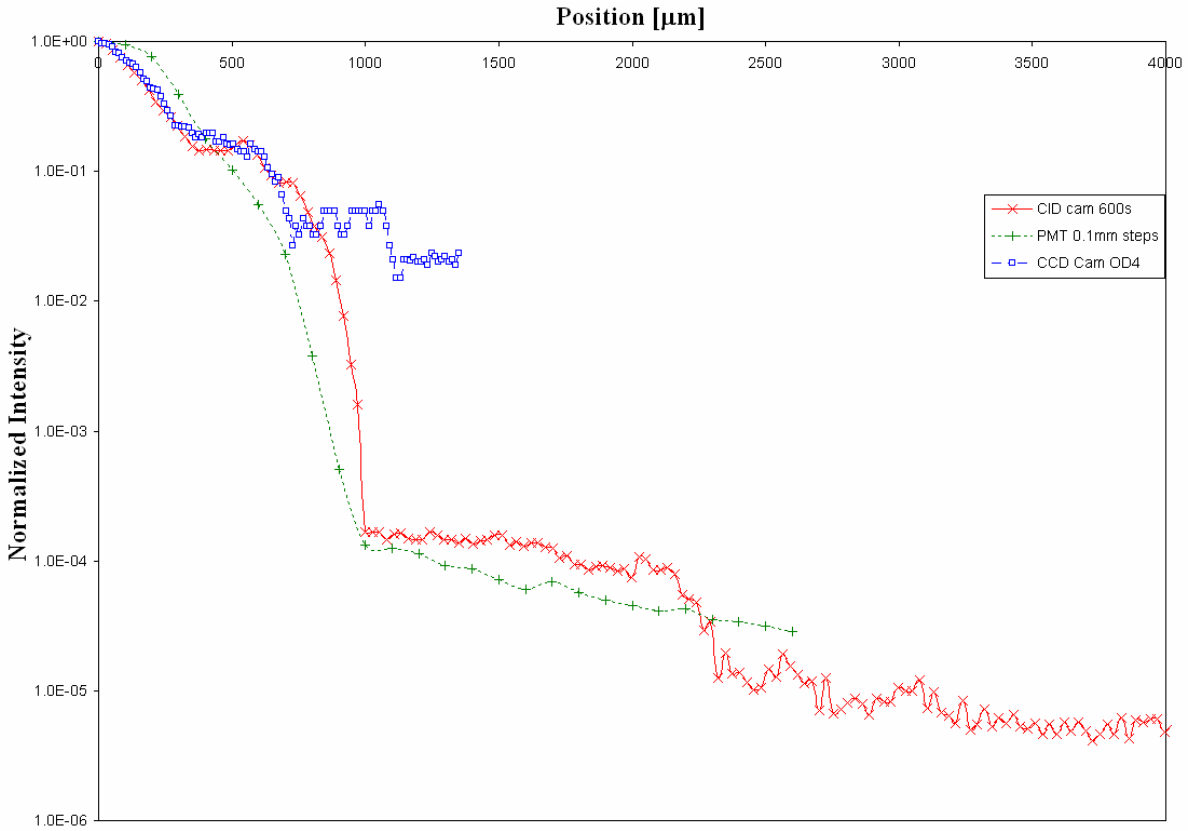

Figure 17: Comparison of the measured intensity distributions with the CCD camera, the SpectraCAM84 and the step-by-step acquisition with the small PMT.

A comparison of the parameters for the three different acquisition methods is shown in Table 1 below. It needs to be pointed out that the PMT can provide a time resolution that even allows intra bunch measurements.

Table 1: Summary of the acquisition parameters of the three different systems

	CCD camera (8 bit)	**PMT setup**	**CID camera**
Pixel Size [μm]	6.5 x 6.25	100 x 100	27 x 27
Dynamic Range	10^2	10^5	10^6
Measurement Time [s]	1	~1800	600
Radiation hardness	Fair	Fair	Poor
Time resolution	~ ms	~ ns	> ms
Cost	$	$	$$

CONCLUSION AND OUTLOOK

The operation of future high intensity accelerators requires a thorough understanding of halo formation mechanisms. This not only implies sophisticated theoretical models and computer code, but also the possibility to explicitly address the issue with experimental techniques. Beam profile measurement techniques based on the exploitation of optical phenomena, such as synchrotron radiation, diffraction radiation or optical transition radiation provide a fast and reliable tool and are already widely used for beam imaging in accelerators around the world. In order to extend the present possibilities, the image acquisition system needs to be able to cover at least five orders of magnitude, which is at the edge of CCD technology. In addition, one would like to have some flexibility, e.g. to limit observation of the beam to interesting regions.

As was shown in this paper, CID technology, and in particular the SpectraCAM® system, paves the way for high dynamic range measurements. Despite existing problems with the control software, the camera system proved to be a reliable tool for profile measurements. Using different pulsed lasers in our optical lab, we realized measurements with dynamic ranges of 10^6 and even beyond without special shielding of background light or the deployment of optical density filters. This is already two orders magnitude better than what is presently required for a more detailed understanding of beam behaviour in CTF3. Improvements seem feasible and future measurement will address OTR related questions in more detail.

ACKNOWLEDGEMENTS

The authors would like to thank Thermo Electron Corporation for the generous loan of the SpectraCAM® system, which made the here-presented measurements possible. Special thanks to Michael J Philon and Tony Chapman for their great support throughout the testing process.

REFERENCES

[1] J.D. Gilpatrick, "Wide Dynamic-Range Beam-Profile Instrumentation for a Beam-Halo Measurement: Description And Operation", AIP CP **693** pp 122 (2003)

[2] P.L. Colestock et al, " The Beam Halo Experiment at LEDA", Proc. Int. LINAC Conf., Monterey, USA, pp806 (2000)

[3] N. Pichoff et al, "CEA Studies on Halo Formation", AIP CP **693** pp 49 (2003)

[4] C. Bovet et al, "The LEP Synchrotron Light Monitors", Proc. IEEE Part. Accel. Conf., San Francisco, USA, pp 1160 - 1162 (1991)

[5] A. Hofmann and F. Meot, "Optical Resolution of BeamCross-Section Measurements by means of SynchrotronRadiation", Nucl. Inst. Meth. A **203**, pp 483 - 493 (1982)

[6] L. Wartski, "Etude du rayonnement de transition optique produit par des électrons d'énergie 30 à 70 MeV. Application aux diagnostics de faisceaux de particules chargées.", Thesis at the Université de Paris-Sud (1976)

[7] D.W. Rule and R.B. Fiorito, “Imaging Micron Sized Beams with OTR”, AIP Conf. Proc. **229** (1991)

[8] M. Castellano, et. al. Phys. Rev. E **63**, 056501 (2001)

[9] A. Potylitsin, Nucl. Instr. Meth. B **145** pp 169 (1998)

[10] M. Castellano and V. A. Verzilov, “Spatial resolution in optical transition radiation beam diagnostics”, PRST-AB **1** 062801 (1998)

[11] V.A. Lebedev, “Diffraction-limited resolution of the optical transition radiation monitor”, Nucl. Instr. Meth. A **372** pp 344 (1996)

[12] X. Artru et al, "Resolution power of optical transition radiation: Theoretical considerations", Nucl. Instr. Meth. B **145** pp 160 (1998)

[13] J.-P. Landragin, "Les capteurs d’images CCD et Cmos", Electronique **137**, pp102 (2003)

[14] http://www.thermo.com

[15] T. Lefevre et al., "Beam Halo Monitoring at CTF3", Proc. EPAC 2004, Lucerne, Switzerland

[16] http://www.vialux.de

[17] G. Michon, H. Burke, "Operational characteristics of CID imager", Solid-State Circuits Conference. Digest of Technical Papers. IEEE International Volume XVII (26) 1974

[18] http://www.hamamatsu.com